Grid impact and power quality assessment of wave energy parks: Different layouts and power penetrations using energy storage

N.B. When citing this work, cite the original published paper.

(article starts on next page)

The Institution of Engineering and Technology WILEY

ORIGINAL RESEARCH PAPER

Grid impact and power quality assessment of wave energy parks: Different layouts and power penetrations using energy storage

Arvind Parwal[1,2] | Johannes Hjalmarsson[1] | Tatiana Potapenko[1] | Sara Anttila[1] | Jennifer Leijon[1] | James Kelly[4] | Irina Temiz[1] | Janaina Goncalves de Oliveira[1,3] | Cecilia Boström[1] | Mats Leijon[1,5]

[1] Department of Electrical Engineering, Division of Electricity, Uppsala University, Uppsala, Sweden

[2] Alstom AB, RCS, HeadQuarters, Marieviksgatan 29, Stockholm, Sweden

[3] Multi-platform Simulations Laboratory, Faculty of Electrical Engineering, Federal University of Juiz de Fora, Juiz de Fora, MG, Brazil

[4] MaREI Centre, Beaufort Building, Environmental Research Institute, University College Cork, Ringaskiddy, Co. Cork, Ireland

[5] Department of Electrical Engineering, Division of Electric Power Engineering, Chalmers University of Technology, Gothenburg, Sweden

Correspondence

Arvind Parwal, Department of Engineering Sciences, Division of Electricity, Uppsala University, Box 65, Uppsala, Sweden 75103, Sweden.
Email: arvindparwal@gmail.com

Abstract

Power fluctuations induced by wave energy converters (WECs) may reflect negative impact on the power quality of the power grid. Assessing their impact is an important step to ensure the grid compliance level of the energy park. The IEC 61000-4-15 standard classifies the allowable disturbances in the grid. This study analysed and assessed the grid impact in terms of flicker, harmonic distortion and voltage variations. The assessments were performed without energy storage and compared when using the energy storage. A single WEC is emulated as an irregular power output of a real WEC using a combined model of power take-off in the Simulink model. Time series based on data obtained in earlier off-shore experiments, conducted at the Lysekil research site in Sweden, is used to emulate a wave energy park (WEP) power in a land-based test rig in real-time power hardware-in-the-loop simulations. A total of three and ten WECs are emulated by introducing a time delay in the time series to investigate the grid impact in each layout. Flicker emissions, voltage variations, individual and total harmonics of the voltage at the connection point in each layout are studied and compared with the limits to be grid compliant for layouts of the WEP. In addition, voltage and current harmonics for the single WEC and individual harmonics in each phase of the voltage are measured and analysed to assess the compliance level of the WEP.

1 | INTRODUCTION

The potential of renewable energy sources (RES) is increasing rapidly and getting recognised as a cost-effective solution for the energy demand [1]. Ocean wave energy is recognised as one of the high potential energy sources to play a vital role for the energy harvesting [2]. Ocean energy is harvested by different means, such as off-shore wind and wave farms [3,4]. Most wave energy technologies are still at early stages [5,6]. The regulatory and economic aspects of wave energy parks (WEPs) have been studied and reported in the literature [7–10]. The power captured by a single wave energy converter (WEC) is highly intermittent due to the nature of ocean waves. This can cause voltage variations in the grid, which, in turn, can affect the power quality, such as flicker and harmonic distortion. In order to reduce the amplitude of the voltage variations, an energy storage can be used to improve the power quality [11] in a grid or microgrid power system. Electrical energy storages (EES) are gaining increased attention due to the increased installation of RES [12]. Microgrids and nanogrids are contributing in terms of price reduction for the consumers and increased revenue for grid operators [13–16]. However, the integration of wave power in the grid requires a thorough assessment in terms of power quality and economic point of view [17]. Literature reviewed [18] presents the grid impact for a low to very high short-circuit ratios and grid impedance angle (Ψ_k) for the WEC operating in fixed mode. However, the study in variable-speed mode for the WEC operation with a microgrid is missing in terms of power

quality context. Therefore, this work filled this gap by analysing the flicker emissions, voltage harmonics and variations at the point of common coupling (PCC) for various power profiles in different layouts connected via a microgrid (400 VAC) power system to the main grid. Moreover, the flicker emissions using an EES and without EES in different power penetrations from the WEP are analysed and compared to the limits, defined in standards IEEE 519-2014 [19] and IEC 61400-21 [20].

1.1 | Power quality in a WEC-connected system

A study on wave energy integration at large scale is presented in terms of transmission constraints in [21]. The performance of several nearshore WECs is investigated and presented in [22]. Due to the fact of intermittent WEC power, the fluctuating power of the WEP induces voltage variations in lower frequency span than wind energy parks [23,24]. This decreases the corresponding flicker severity of the WEP in terms of flicker perceptibility as reported in the IEC report [25]. Most of the fluctuations occurred ranges between 0 and 10 Hz. In spite of the lower frequency range, the voltage variations present higher amplitude on the short timescale of seconds. Hence, increased flicker of the voltage causes increased total harmonic distortion (THD) at the PCC. In addition, WEPs use long power cables around a few kilometres, whose capacitance induces a reactive power generation/consumption, which influences the voltage. To be able to comply with the grid code requirements, these issues have to be resolved. In order to assess these aspects for an improved power quality and grid code compliance [19,20], a grid impact assessment needs to be done. Grid impact generated by a WEP for flicker analysis and voltage variations at the PCC depends on the ratio of the short-circuit level of the local power grid to the WEP maximum power [26]. However, the layout and aggregation of the WEC-based energy park has a noticeable impact on power quality [27]. Aggregation of the WEC devices in different layouts, such as fixed and randomly distributed, has an impact on the lower EES cost and on fluctuations in the power production. The evaluation of such layouts can be done by shifting the time series of a WEC with certain time delays.

This paper considers the time series of WECs aggregated in three different layouts. The first layout consists of a single WEC. The other two layouts consist of three WECs and 10 WECs. The time series is shifted by a time delay of 0 and 10 s for three-WEC aggregation. The aggregation of 10 WECs is done in a fixed and a random distribution. The potential grid impact in various WEP layouts is assessed in a microgrid for the power quality assessment. The contribution of short-term flicker severity is analysed using the methodology defined in the standard IEC 61400-21 for a fictitious grid with a grid short-circuit ratio equal to 50. The study is carried out under the framework of MaRINET2, European Union framework. The tests were conducted at the Centre for Marine and Renewable Energy Ireland (MaREI), Cork, Ireland, in 2018.

The rest of this paper is structured as follows. Section 2 presents an overview of the system and the specifications of
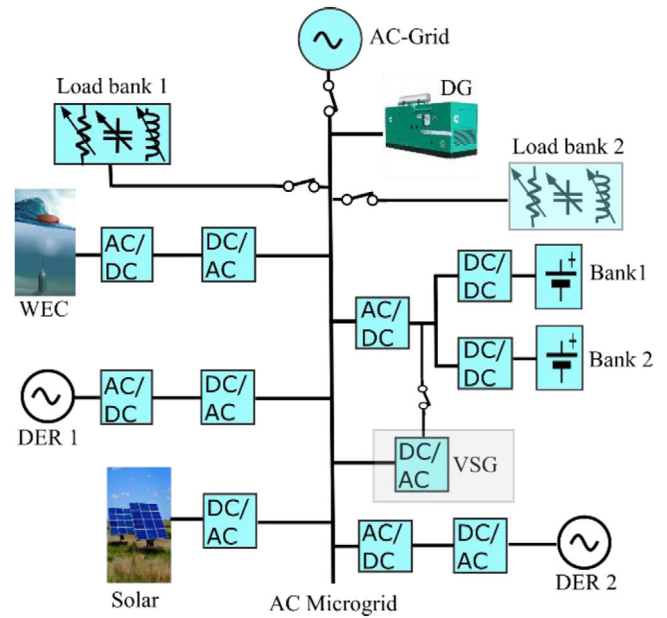

FIGURE 1 Structure of AC microgrid at MaREI facility [28]

each layout in details. In Section 3, the methods for the estimation of flicker emissions, voltage variations and the harmonics at the PCC are discussed in detail. Section 4 presents the analysed results and discussion, and Section 5 discusses the summary of the results as the potential findings of this work. Finally, this paper is concluded by presenting a detailed conclusion in Section 6.

2 | SYSTEM DESCRIPTION

The WEC devices are connected to a microgrid, as shown in Figure 1, where the extracted power from the RES is interfaced with the main utility.

2.1 | Power hardware in the loop in wave power application

Hardware-in-the-loop (HIL) systems usually consist of a physical controller combined with a virtual plant executed in real-time (RT) computer simulations. RT simulations with HIL allow us to test the controller at earlier development stages, to discover eventual design issues at different operational—including faulty and extreme—conditions, to replace risky and expensive physical tests and, thereby, to reduce the development costs. A detailed discussion of the system structure can be found in [28]. In order to investigate the grid impact in different power levels and layouts, the WECs are clustered in three layouts as shown in Figure 2.

- *A*: single WEC; see Figure 2(a).
- *B*: three WECs connected with two different time shifts, 0 and 10 s, see Figure 2(a).
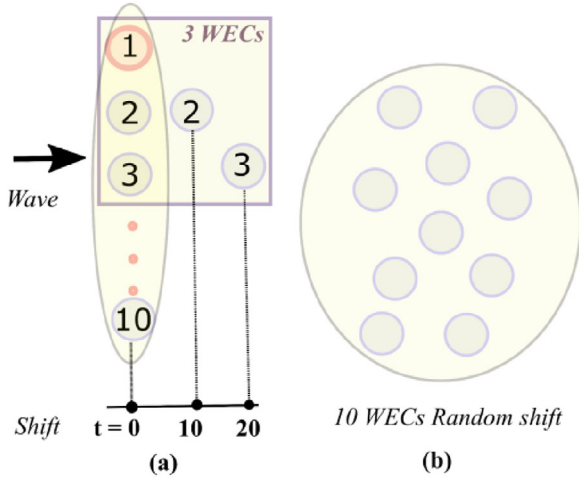
FIGURE 2 Overview of the layouts of the WEP. (a) A squared showing a single-WEC- and three-WEC-based layout for 0–10-s shifts and 10-WEC-based layout for a fixed shift. (b) Showing a random shift for 10 WECs

- *C*: 10 WECs connected with two shifts, fixed and random; see Figure 2(a) with zero shift and Figure 2(b).

In order to assess the behaviour of a WEC, a single WEC case is studied, where the power production is highly intermittent for a specific sea state. The generator was operated in variable-speed operation and interfaced with the microgrid. In Figure 2, the WEC is represented by a circle. *Layout A* consists only one WEC represented as an orange circle, shown in Figure 2(a). This layout is considered as a scenario where a highly intermittent power is injected. A single WEC is performing for a considered sea state typical at Lysekil research site on the west coast of Sweden [29,30]. A detailed description of the WEC model and power take-off (PTO) can be found in [31]. A significant wave height H_s of 2 m and an energy period T_e of 6 s are used in the experiment. The WEC data is sampled at 0.01 s of resolution. The WEC is interfaced with the grid, and voltage fluctuations at the PCC are sampled for more than 600 s to evaluate the flicker emissions. However, a single WEC grid-connected case can never be a recommended case in a commercial application. The investigation in this case was focused on the WEC behaviour with the microgrid only. In *Layout B*, three WECs are represented in a squared orientation, where a zero shift is defined by $\Delta t = 0$, all the WECs are facing the same wave. Also, the shift $\Delta t = 0$ is applicable to the fixed shift for 10 WECs in *Layout C* and represented by an oval shape, as shown in Figure 2(a), whereas a 10-s shift is applied by modelling $\Delta t = 10$ for three WECs in *Layout B* as represented in a squared orientation. *Layout C* for randomly connected 10 WECs is represented in Figure 2(b). Small blue circles represent individual WECs in *Layouts B* and *C*. The power pulsations occurred by the WEP are comparatively smaller than wind energy parks [25]. The layout selection for *Layouts B* and *C* is based on two aspects to study: WEC orientation and minimum fluctuation. A grid-connected converter is shown in Figure 3, where the power is injected to the PCC. The power from the WEC(s) is injected to the DC bus, which serves as an isolation for the WEC and
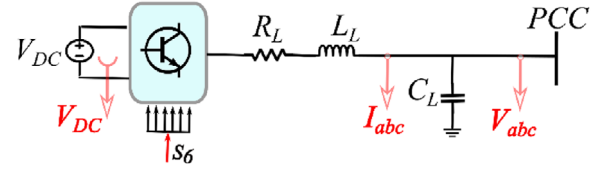

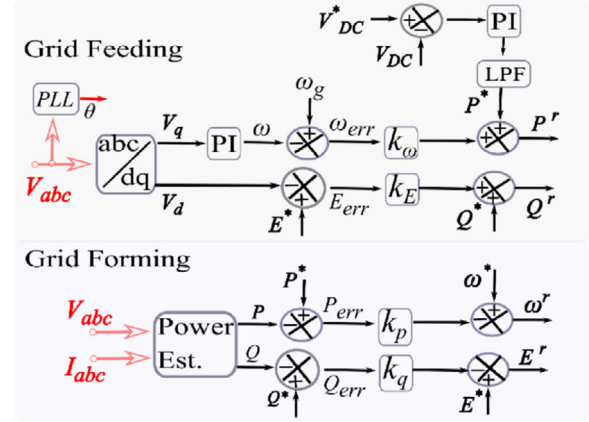**FIGURE 3** Overview schematic of a grid-connected VSI

FIGURE 4 Generation of referenced variables in grid-connected and islanded modes

grid side converters. The voltage-source inverter (VSI) is connected to the PCC through an LC filter, where L_L and C_L are the filter inductance and capacitance, respectively. V_{DC} is the measured DC-link voltage used in voltage regulation loop and is discussed later.

2.2 | Control of a power converter

This section presents the control of a microgrid-connected VSI in the grid-connected mode using a proportional- resonant (PR) controller. The VSI is controlled to maintain a balanced symmetry of three-phase voltages in the microgrid under grid operating and islanded conditions. Besides a voltage regulation at the DC link, the VSI is also tasked to perform other functions such as proper dispatch of active and reactive power, a smooth synchronisation of the micro and utility grid during the transition from grid-connected (grid-feeding) to islanded (grid-forming) mode. A control structure used for generation of referenced variables for voltage and current regulation is shown in Figure 4. The study presents results from a grid-connected system point of view. Hence, the control of the VSI in an islanded mode is not discussed.

In a grid-feeding mode, the three-phase voltages at the PCC are used to track the grid phase using a phase-locked loop and generate the *dq*-axis voltage variables, V_{dq}. A tuned PI regulator is used to generate the angular frequency ω from the variable V_q and is compared to the grid frequency ω_g. The error ω_{err} from the comparator is regulated by using an active gain parameter k_ω and the resultant is summed up with the referenced variable
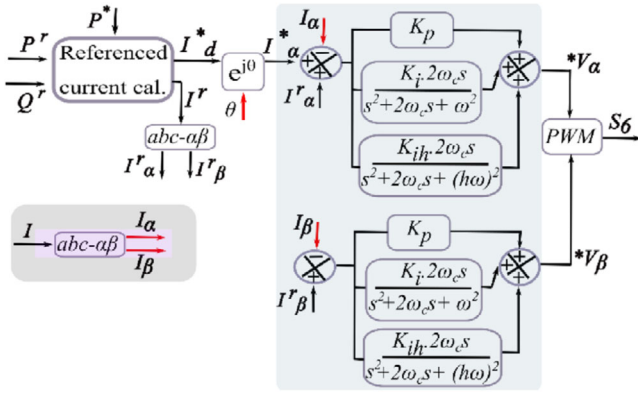
FIGURE 5 Three-phase grid inverter control using the PR + HC controller

FIGURE 6 Open-loop Bode diagram of the PR controller with the HCs

P^* from the voltage regulator. The total sum P^r is the referenced variable for the active power to be compensated by the VSI. The referenced variable P^* is generated by a PI regulator and filtering the output using a low-pass filter. The reactive power referenced variable Q^r is generated using a reactive gain parameter k_E. These referenced variables are fed to the current control loop to generate the referenced voltage variables to the pulsewidth modulator to control the insulated-gate bipolar transistor switches of the VSI.

2.3 | Current control in a grid-connected mode

A PR current control strategy with harmonic compensator (HC) is used to control the power flow and eliminate the lower-order odd harmonics in the microgrid, as shown in Figure 5. The ideal PR current controller is represented as [32]

$$G_{PR}(s) = K_P + K_i \frac{s}{s^2 + \omega^2} \tag{1}$$

where K_P is the proportional gain, K_i is the integral gain and ω is the resonant frequency. This makes the ideal PR system controller with an infinite gain at the frequency of ω and no phase shift and gain at other frequencies. To avoid the stability problem related to an infinite gain, the PR controller can be made non-ideal by introducing damping as shown in the following equation:

$$G_{PR}(s) = K_P + K_i \frac{2\omega_c s}{s^2 + 2\omega_c s + \omega^2} \tag{2}$$

where ω_c is the bandwidth around the AC frequency of ω. From (2), the gain of the PR controller at the AC frequency ω is now finite, but it is still large enough to provide only a very small steady-state error. This equation also makes the controller more easily realisable in digital systems due to their finite precision.

2.3.1 | HCs with PR control

The additional non-ideal HC $G_H(s)$ with PR control is shown in (3) and shown in Figure 5. The non-ideal $G_H(s)$ is implemented,
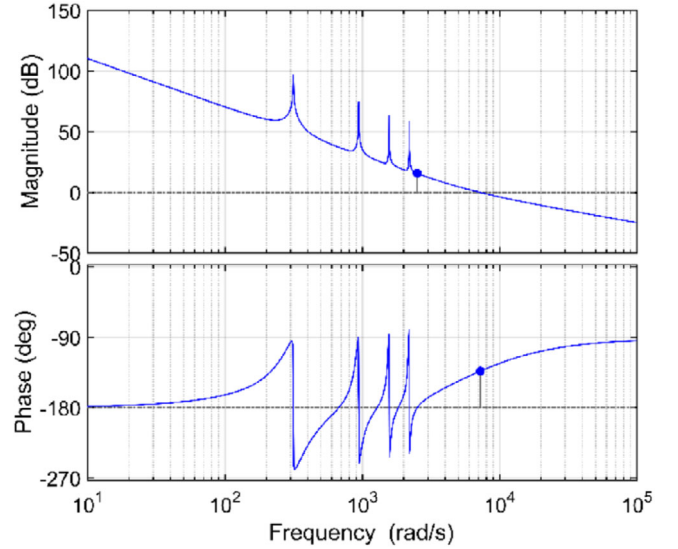
instead an ideal HC due to the stability problem with infinite gain as stated for the PR controller

$$G_H(s) = \sum_{h=3,5,7} K_{ih} \frac{2\omega_c s}{s^2 + 2\omega_c s + (h\omega)^2} \tag{3}$$

where K_{ih} is the resonant gain at the particular harmonic, $h\omega$ is the resonant frequency of the particular harmonic and ω_c is the bandwidth around the particular harmonic frequency of $h\omega$.

The third-, fifth- and seventh-harmonic compensators are designed at individual resonant frequency by choosing ω_c and K_i at 3ω, 5ω and 7ω, respectively. The transfer function of complete controller $G_C(s)$ is defined

$$G_C(s) = G_{PR}(s) + G_{3H}(s) + G_{5H}(s) + G_{7H}(s). \tag{4}$$

The parameters used in the control are presented in Appendices.

The open-loop bode plot of the system is presented in Figure 6, where the obtained gain margin is 15.7 dB at 2.51 krad/s and the obtained phase margin of 46.7 at a frequency of 7.24 krad/s. It is evident form Figure 6 that the selective harmonic compensation is achieved by the cascaded compensators at 3ω (150 Hz), 5ω (250 Hz) and 7ω (350 Hz) frequencies.

3 | GRID CODE COMPLIANCE: FLICKERS, HARMONIC DISTORTION AND VOLTAGE VARIATIONS

Flickers, impression of unsteadiness of visual sensation by a light stimulus, may cause severe damages in the power system and to the persons in the community [33]. In order to determine the permitted levels and the limits of the flickers, regulated by the standards IEC 61000-3-7 [32] and 61400-21, it can be analysed either as the maximum contribution of the plant or

to the total flicker level at the PCC. The current IEC regulation enforced in terms of short-term flickers, P_{st}, analysed over 10 min operation and long-term flicker emissions, P_{lt}, ensures the safe operation for the power systems, which is considered below 0.35 for a plant to be compliance as grid operator requirements in Ireland [34], whereas this limit is slightly relaxed to unity in case of Sweden [35]. A WEP can be considered compliant if the flicker emissions induced at the PCC are below 0.35 [17]. Several studies have been reported in the literature, where the potential grid impact induced by a small- to medium-size WEP is investigated [36–38]. The standard IEC 61400-21 defines a procedure method for flicker emissions, where fictitious grid (represents the interaction between the WEP and the grid) short-circuit apparent power (S_k) is 50 times the rated apparent (S_p) power of the WEP. The grid characteristics are determined as follows [39]:

$$S_k = \frac{U_n^2}{\sqrt{R_k^2 + X_k^2}} = \frac{U_n^2}{Z_k} \qquad (5)$$

$$\Psi_k = \arctan\left(\frac{X_k}{R_k}\right) \qquad (6)$$

where U_n is the grid voltage and R_k, X_k and Z_k are the fictitious grid resistance, reactance and impedance, respectively. The ratio in (6) determines the grid impedance angle (Ψ_k). The short-circuit ratio (S_k/S_p) and the impedance angle of the grid define the grid strength of a small- or medium-size WEP. A low value of grid strength would impose a problem in terms of flickers. This factor may cause higher voltage variations due to a single WEC operation or lower level of grid strength. However, an aggregation of several WECs in a group and groups into a park would resolve the problem of flicker emissions [18,40]. Moreover, a significant reduction in the individual short-term flicker level and, hence, a reduced total flicker emissions can be achieved as required by the IEC standard, if EES is used in the system. The EES provides a reduction in the amplitude variation at the PCC voltage. If the flicker level ranges between 0.35 and unity, the WEP is considered compliant to a grid-connected operation as per flicker limits are assigned [33]. However, if the flicker limits are violated and exceed 1.0, the WEP does not comply with the requirements. Flicker levels are affected inversely to the grid impedance angle Ψ_k; a high impedance angle reduces the level of flickers. A grid impedance angle of $\Psi_k = 85°$ will not get affected by flicker exceeding values. In this study, the work is focused in three aspects to present an operational grid integration: flicker emissions, harmonic distortion and voltage fluctuations at the PCC.

3.1 | Flicker emissions

The flicker level at the PCC can reach to a higher value in a worst-case scenario, such as a weak grid (lower short-circuit ratio) and WEP layout (high power fluctuation). The minimum short-circuit ratio recommended for lower and slightly higher Ψ_k points at 30° and 50° is 6 and 4, respectively [17]. This

values is preventing flicker level to exceed 1.0, whereas points with higher grid impedance angle (70°, 85°) are not much affected by considering their high short-circuit ratio. For the most stringent limit ($P_{st} = 0.35$), the short-circuit ratio increases above 20. A wind farm is recommended for a connection with a short-circuit level of 25 or a suitable power factor control with lower short-circuit level [41,42]. The standard IEC 61000-4-15 defines two observation periods:

(i) short term, assessed for fixed 10 min, which assessed the short-term flicker severity, P_{st};
(ii) long term, assessed for 2 h, for the long-term flicker severity, P_{lt}.

The instantaneous sensation of flicker may be subject to strong and non-linear variations. Therefore, individual levels exceeding during the observation time must be taken into account [43]. The short-term flicker (P_{st}) can be obtained as follows [43]:

$$P_{st} = \sqrt{k_1 P_1 + k_2 P_2 + k_3 P_3 + \cdots + k_n P_n} \qquad (7)$$

$$\left.\begin{array}{c} P_1 = P_{0.1} \\ P_2 = P_{1s} = \dfrac{P_{0.7} + P_1 + P_{1.5}}{3} \\ P_3 = P_{3s} = \dfrac{P_{2.2} + P_3 + P_4}{3} \\ P_4 = P_{10s} = \dfrac{P_6 + P_8 + P_{10} + P_{13} + P_{17}}{5} \\ P_5 = P_{50s} = \dfrac{P_{30} + P_{50} + P_{80}}{3} \end{array}\right\} \qquad (8)$$

where $k_{1\ldots n}$ are weighting coefficients and $P_{1\ldots n}$ are levels corresponding to the percentiles 1, 2, …, n. The results are evaluated based on (7) for $\{k_1, k_2, k_3, k_4, k_5\} = \{0.0311, 0.0125, 0.0246, 0.027, 0.071\}$.

In (8), where the index s refers to averages, $P_{0.1}$ is the instantaneous sensation value of flicker exceeding during a 0.1% observation time. The long-term flicker severity (P_{lt}) is based on the cubic geometric average of 12 values of P_{st} for 120 min and can calculated as

$$P_{lt} = \sqrt[3]{\frac{1}{12} \sum_{i=1}^{12} P_{st,i}^3}. \qquad (9)$$

The flicker coefficient (c_f) is computed from the voltage variations at the PCC during the WEP operations as

$$c_f(\Psi_k) = P_{st} \frac{S_k}{S_p}. \qquad (10)$$

3.2 | Total harmonic distortion

Voltage and current harmonics are expected to appear with the interfacing of power electronics converters and non-linear

loads. The levels of harmonics allowed in the Swedish grid are regulated in [44]. The parameters measured for the comparison in three different layouts are analysed according to the limits described in EN 50160 and IEEE 519-2014 at the PCC. The standard states the limits for THD and the peak limits of the individual voltage and current harmonic and is calculated in (7). The allowed 10-min voltage THD for the low-voltage network (≤ 1.0 kV) is 8% calculated for the 95th percentile value, whereas the individual harmonic limit is defined as 5% in both European standard EN 50160 and the IEEE standard 519-2014. However, the THD limit for the 99th percentile short-time values, measured for 3 s, should be 1.5% times less than the values mentioned for individual and the THD for low-voltage network, as defined in IEEE 519-2014 [19]. The current distortion limits for individual odd harmonics for systems rated 120 V through 69 kV for the 95th percentile (very short time—3 s) and the 99th percentile (short time—10 min) values are corresponding to the ratio of the short-circuit current I_{SC} and maximum demand current I_L at the PCC [19]. For $I_{SC}/I_L = 50 < 100$, the odd harmonics limit ($3 \leq h < 11$) is set to 10%, and the even harmonics are limited to 25% of the defined odd harmonic limits

$$\left.\begin{array}{c} \text{THD}_v = \dfrac{\sqrt{\sum_{h=2}^{N} (V_h)^2}}{V_1} \\[4mm] \text{THD}_i = \dfrac{\sqrt{\sum_{h=2}^{50} (I_h)^2}}{I_L} \end{array}\right\} \qquad (11)$$

where h is the order of the harmonic, and V_1, and I_L are fundamental component of the voltage and maximum demand current at PCC. The voltage THD, individual odd harmonics third to ninth and even harmonics fourth to eighth in the voltage and currents at the PCC are studied.

3.3 | Voltage level

The amplitude of the voltage variation ΔV at the PCC is computed as follows [45]:

$$\Delta V = \frac{PR + QX}{V} = \frac{PR}{V} \text{ when } P \gg Q \qquad (12)$$

where P is the active power and Q is the reactive power at the PCC. R and X are the resistance and the reactance of the grid, respectively.

4 | RESULTS AND ANALYSIS

In this section, the results from the layouts considered during the study are presented. The results are presented in terms of the flicker emissions, THD of voltage and current, and the voltage variations at the PCC.
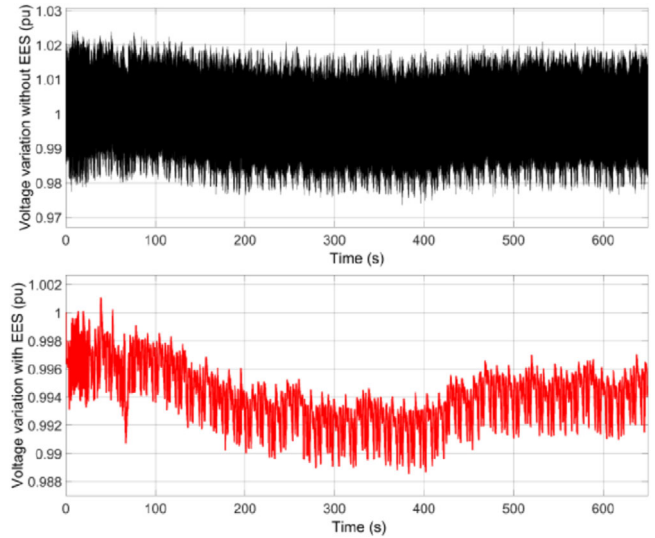

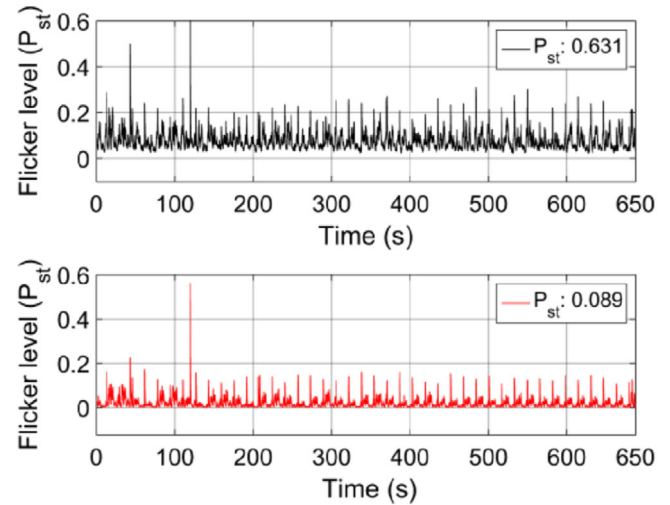**FIGURE 7** Voltage variation; black curve without EES and the red curve with EES

FIGURE 8 Flicker level P_{st}; black curve shows without energy storage and red curve shows when energy storage is used

4.1 | Layout A: Results analysis of a single WEC

Figure 7 shows the voltage variations by the equivalent electrical power time series, which would be the output by a WEC for the production period considered. Figure 8 shows the flicker levels for the WEC power without the energy storage in black curve and with the energy storage in the red curve. It can be noted from the results that the power captured from a single WEC directly delivered to the power grid, resulting higher fluctuations in the voltage variations at the PCC. It is worth to mention that the grid impedance angle Ψ_k at the connection point of the microgrid is 70°. The evaluated flicker level P_{st} is 0.631, which is significantly higher than the IEC requirement of 0.35 for short-term flicker emissions. This is due to the higher
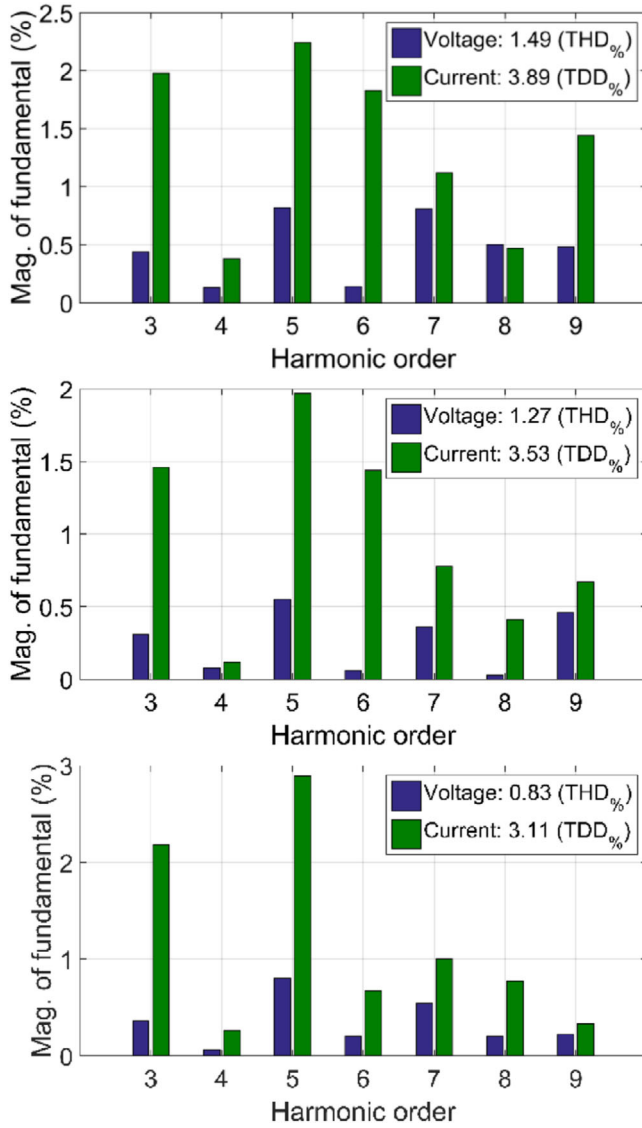
FIGURE 9 THD of the grid voltage in the blue and current in the green colour at 20, 100 and 200 s, top to bottom, respectively. The voltage and current THD/TDD at the observed time instants are below the limit allowed in EN 50160 and IEEE 519-2014

fluctuation at the PCC voltage induced by the single power generating unit. Thus, it is not favourable to connect a single WEC to the power grid. However, the short-term flicker level (P_{st}) is significantly decreased to 0.089 when using energy storage, as shown in the red curve in Figure 8. For the THD measurements, the data logged for 10 min are evaluated at different time instants to investigate the THD of the voltage and the current in a variable-speed operation. Therefore, it is crucial to determine the THD at different time periods in a single-WEC-connected case. The THD in the voltage, currents, and in each phase of the voltage at the PCC at 20 s, 100 s and 200 s of time instants is investigated when the energy storage is used. Figure 9 presents the THD contents in the voltage and the current at different time instants.

It is evident that the odd harmonics third to ninth and even harmonics fourth to eighth do not surpass the limit defined in either EN 50160 or IEEE 519-2014. The odd harmonics in the voltage present a reduction for the observed time periods, where fourth and eighth voltage harmonics show a reduction in the harmonic content at 20 and 200 s, respectively, while the sixth-order harmonic stays almost the same and reduced at 100 s as in the blue bar plotted and shown in the middle graph in Figure 9. The total demand distortion (TDD) is considered for the currents at the PCC. The results satisfied the individual harmonic limits: <10% for odd harmonics and 25% of 10% limit for even harmonics for the 95th percentile short time values, and less than two times for the 99th percentile very short time values, as defined by IEEE 519-2014.

The odd harmonics third, seventh and ninth show a reduced magnitude, whereas fifth harmonic shows an increment the magnitude of the fundamental. The odd harmonics remained below the maximum allowed limit, and the even harmonics are noticeably below the limit of 25%, as defined in IEEE 519-2014. The voltage THD at 20-s time observed period is almost 1.5%, which is far less than 5.33%, 1/1.5 times the limit value of 8%. However, the THD is much reduced for the 95th percentile short-time values at 200 s to a THD of 0.83%, as shown in Figure 9 (bottom plot). The fundamental component of the signal is at 50 Hz and the sampling frequency was set to 3 kHz.

4.2 | Layout B: Results analysis for three WECs with zero shift and 10-s shift

During the tests, three WECs were considered as a group in the WEP and each WEC was modelled as a controlled current source with a zero shift. In this case, the captured power from the three WECs fluctuates simultaneously (i.e. the same wave impacts equally). In the case of grouped WECs, the power delivery is rather smoother when compared to a single-WEC case. Therefore, the results are presented in terms of short-term flicker emissions and power and voltage spectra along with the individual harmonics of the voltage. The power fluctuations induced by the WECs continuously fluctuate the magnitude of the amplitude, and using EES, these occurrences of often fluctuations are reduced up to a great extent. The smoothened peak powers from the layouts are 51 and 30 kW for zero and 10-s shift, respectively, as shown in Figure 10. Figure 11 presents the short-term flicker level (P_{st}) without EES in the black curve and in the red curve when the storage is used for zero and 10-s shift. The P_{st} was found almost to 0.112 with the three-WEC 10-s shift powered case at the PCC. The P_{st} level is reduced to 0.021 when the EES was used. However, flicker level P_{st} in the zero-shift case was noticeably higher when compared to 10-s shift. The power and voltage spectra are evaluated to determine the power pulsations and presented in Figure 12 for zero and 10-s shift. The spectra of power and voltage clearly show that the frequency range of the voltage fluctuations occurred by the WEP in zero and 10-s shift is comparatively much smaller than wind energy parks and also in a single-WEC case. In
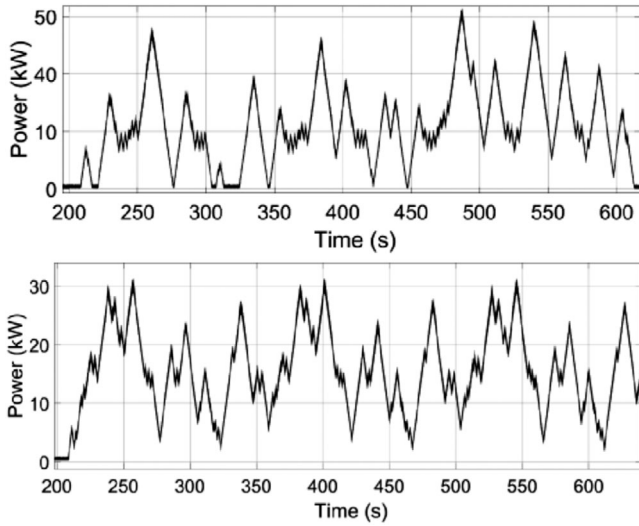
FIGURE 10 WEP power profiles for zero (upper plot) and 10-s shift (lower plot) for three WECs
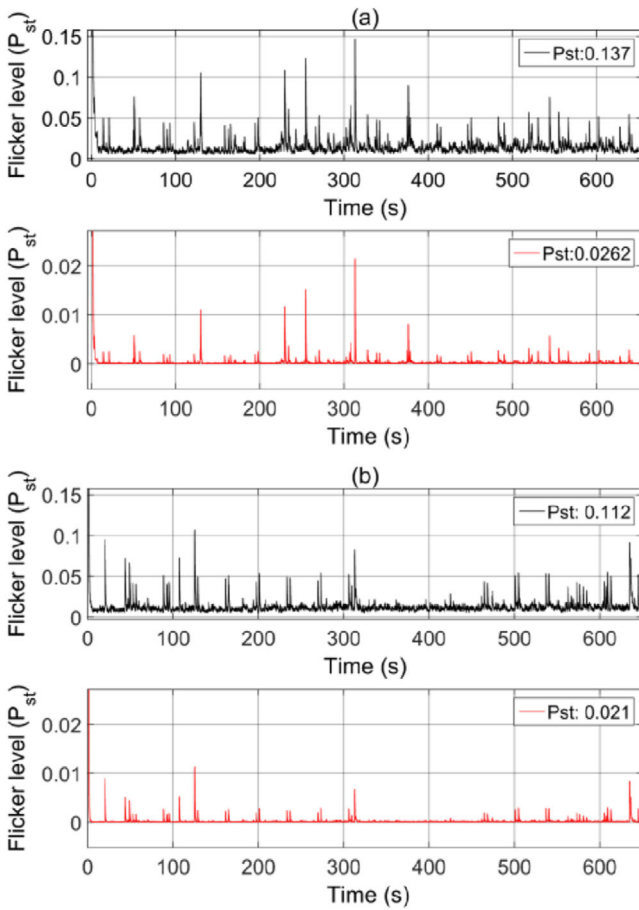

FIGURE 11 Flicker level P_{st} of three WECs. (a) Three WECSs with zero shift. (b) Three WECs with 10-s shift. Black curve shows without energy storage and red curve shows when energy storage is used
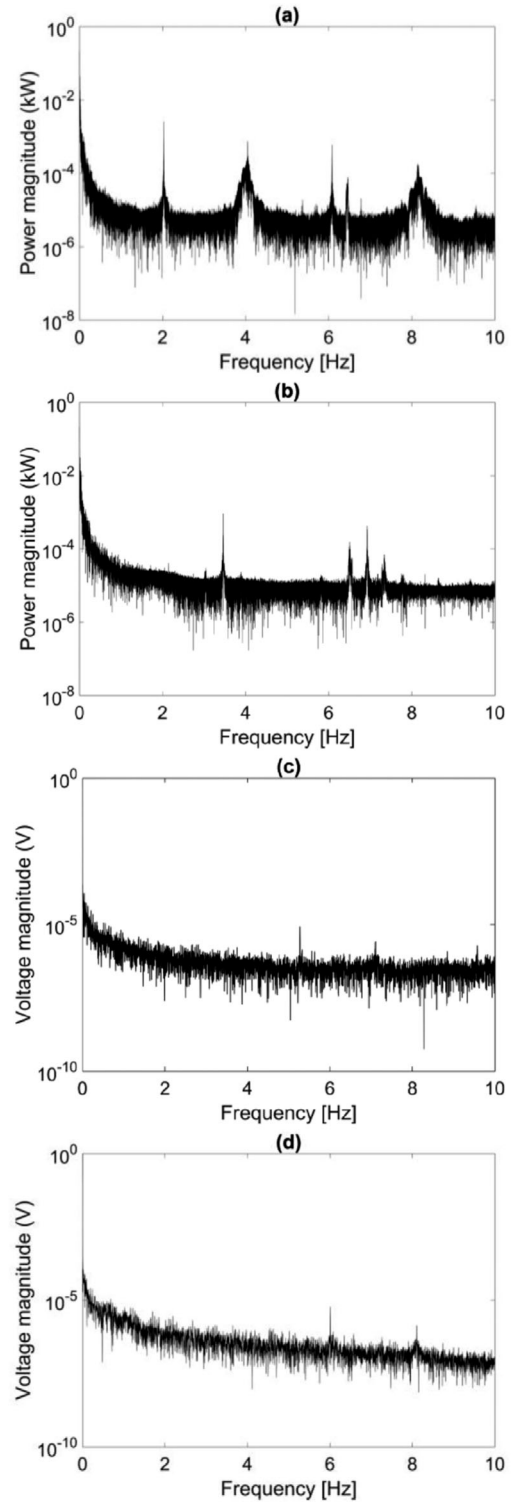
FIGURE 12 Spectra analysis for three WECs in zero and 10-s shift with energy storage. (a) and (c) Spectra of the power and voltage in zero shift. (b) and (d) Spectra of the power and voltage in 10-s shift (All measured in pu.)

power spectra, the power fluctuations are more often occurred between 2 and 10 Hz of frequency.

Although both the cases investigated are fairly compliant as per IEC requirement regulated for the WEP, it is worth to mention that the grid impedance level and short-circuit ratio would

FIGURE 13 Individual odd harmonics (third to ninth) of the voltage for three WECs with EES. (a) Zero shift. (b) 10-s shift

FIGURE 14 Flicker level P_{st} of 10 WECs. (a) 10 WECSs with fixed shift. (b) 10 WECs with random shift. Black curve shows without energy storage and red curve shows when energy storage is used
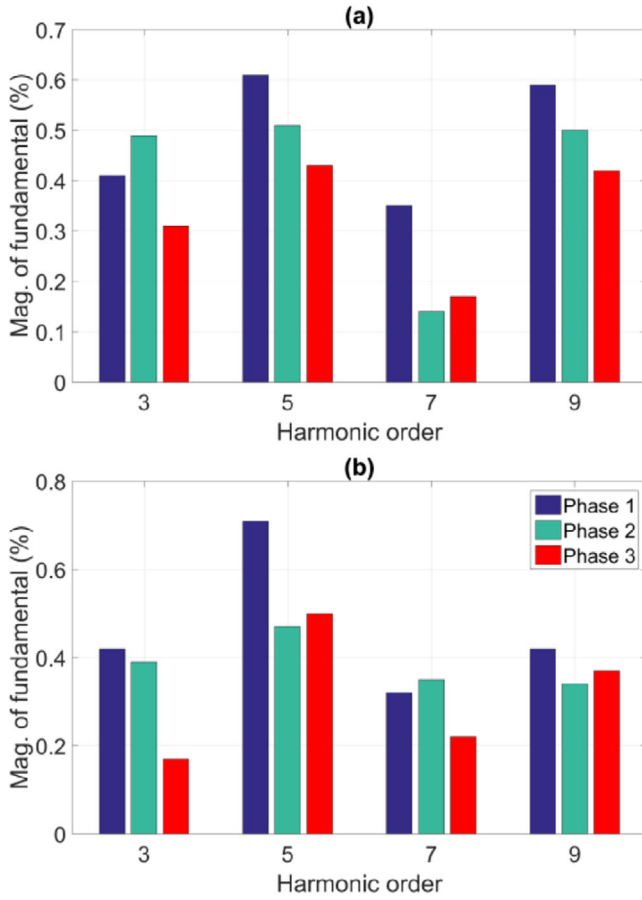
affect the P_{st} level. Since the considered cases show lower values of flicker level $P_{st} = 0.0262$ and $P_{st} = 0.021$ for zero and 10-s shift, the voltage spectra show a reduced fluctuation in the amplitude of variations if compared to the single-WEC case. The outcome of the results fairly meets the IEC-compliant requirements for the three-WEC-based WEP. However, the voltage harmonics would appear in both the cases; therefore, harmonics at the PCC in zero and 10-s cases are investigated and presented with their individual magnitude of fundamental for each phase of the voltage in Figure 13. Figure 13(a) and (b) shows the individual harmonics calculated at the PCC voltage and evaluated as per the IEEE 519-2014 standard requirement for zero and 10-s shift. The odd harmonics in individual phases, in zero and 10-s shift, are reasonably below the limits allowed. In 10-s shift, the third harmonic is significantly reduced in all the three phases. However, the fifth harmonic in phase 1 was increased in the 10-s shift case [see Figure 13(b)], while the other two phases show a reduction in the harmonic amplitudes. The seventh-harmonic amplitudes for individual phases 2 and 3 have increased a bit in 10-s shift, whereas seventh harmonic in phase 1 presented a marginal reduction. Ninth harmonic has been reduced significantly in all the three phases. The slight variation in individual phases is due to the variation in the voltage and fairly compliance as per the IEC standard requirements even
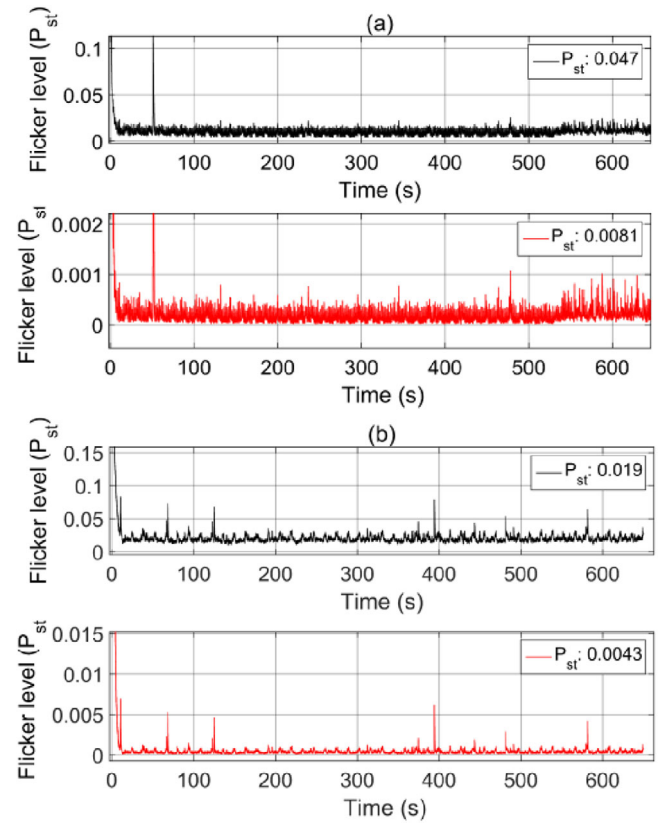
compensated using EES. Moreover, the results from *Layout B* confirmed that the compliant level of three-WECs cases is satisfied without EES. Moreover, the results presented are applicable to any type of generator connected through this interface, grid impedance angle, and short-circuit ratio. It should be noted that the short-circuit ratio and the grid impedance angle were 50 (S_k/S_p) and $\Psi_k = 70°$, respectively, in the tests conducted at the MaREI Centre.

4.3 | Layout C: Results analysis for 10 WECs with fixed and random shift

In this layout, a total of 10 WECs are considered in a WEP as DER 2, as shown in Figure 1. The distribution of 10 WECs is considered in two configurations: fixed and random. In the first case, all of the WEC power profiles are in phase with the others; this leads to a condition where all WECs are almost facing the same wave at the same time, similar to a zero shift case in previous section. The latter case has none of the power profiles in phase, which leads to a smoother power output from the WEP. In order to investigate the grid impact, the tests were performed for short-circuit ratio as in previous tests. Flicker levels for fixed and random layout are presented in Figure 14. In Figure 14(a) and (b), the results present the flicker severity in fixed and random orientation of 10 WECs without EES

and using EES, respectively. From the results, it is evident that this layout for random shift fairly satisfied the grid code compliance for flicker severity. The grid impact with 10 WECs in fixed orientation presents a flicker level $P_{st} = 0.047$ without smoothing the power, as shown in Figure 14(a). When the WEP power is smoothed and interfaced with the grid, the flicker level is reduced to 0.0081 for the observed time period. Figure 14(b) shows the reduced level of flicker $P_{st} = 0.019$ (no EES) and $P_{st} = 0.0043$ (with EES) for the random orientation of the WECs. The power pulsations and voltage variations in both orientations are presented in Figure 15 when EES is used. Figure 15(a) and (b) shows the power variations in fixed and random WEC selection, respectively. The power variations are often occurred in a fixed case where all the WECs capture the power from the same wave. As expected, the magnitude of variations is smoothen out when compared to three-WEC 10-s results, since the power delivery has increased in 10 WECs layout for fixed and random both. Due to this fact, small variation can be seen around 6 and 10 Hz in Figure 15(a).

It can be noted that the amplitude of these variations has reduced to a noticeable amount. Figure 15(b) presents the power pulsations in randomly distributed WECs. Variations shown, between 2 and 10 Hz, are reduced to 50% of fixed distribution. The voltage variations for fixed and random orientation are shown in Figure 15(c) and (d). In randomly distributed WECs, the voltage variations are significantly reduced, which provided a favourable condition for a safe and improved power quality operation. This condition of attenuation has reduced the flicker severity, amplitude of the voltage variation and the harmonic distortion at the PCC. In order to determine the harmonic content at the PCC, individual harmonic amplitudes are analysed at the PCC voltage and presented in Figure 16 for fixed and random orientation with EES. The results from Figures 14–16 stated that the flicker emissions are greatly reduced compared to the non-smoothed power. All values of short-term flicker severity are below 0.25, which follows the limit specified in the IEC standard.

5 | SUMMARY OF THE RESULTS

The results presented in *Layouts A, B* and *C* in terms of flicker emissions, voltage and power variations have demonstrated the behavior and applicability of the WEP to be compliant to the IEC and IEEE 519-2014 standards. The results from *Layout A, B* and *C* determined their individual grid impacts at the PCC, as shown in Figure 17. *Layout A* shows a severe flicker level for a single WEC without EES, which ranges to $P_{st} = 0.631$, whereas this severity has been significantly reduced to $P_{st} = 0.089$ when using EES. Therefore, a single WEC without an energy storage is not compliant to IEC standards IEC 61400-21 and 61000-4-15. This is the case when only single WEC is operating and injecting a highly fluctuating power, which leads to higher voltage variations at the PCC. The short-term flicker level in *Layouts B* and *C* with different orientation has been reduced and remained below the limits allowed. The flicker level, P_{st}, of *Layouts B* and *C* confirmed that the grid impact level
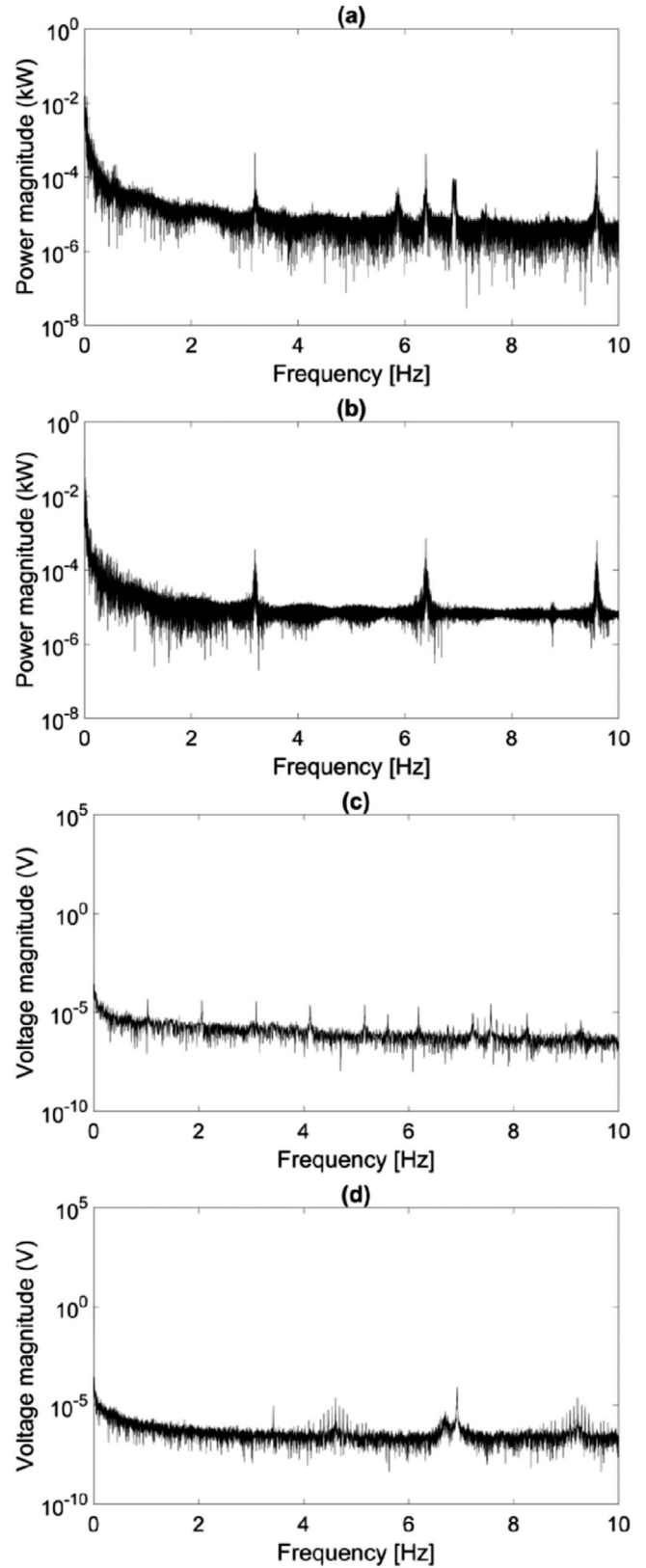

FIGURE 15   Spectra analysis for 10 WECs with energy storage. (a) and (c) Spectra of the power and voltage in fixed orientation. (b) and (d) Spectra of the power and voltage in randomly distributed orientation (All measured in pu.)
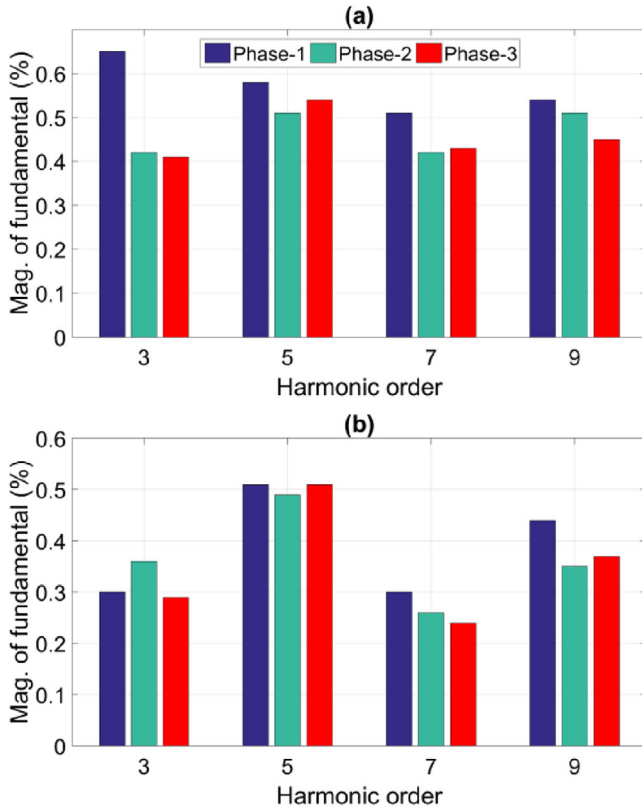
FIGURE 16 Individual odd harmonics (third to ninth) of the voltage for 10 WECs with EES. (a) Fixed shift. (b) Random shift
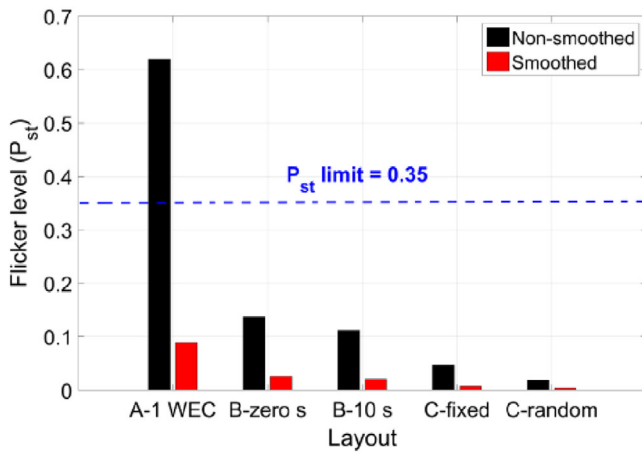

FIGURE 17 Grid impact in terms of short-term flicker level for each layout and time shifts

TABLE 1 Maximum voltage variation ($\Delta V / V$) for each layout in %

	A One WEC	**B—three WECs**		**C—10 WECs**	
		Zero shift	**10-s shift**	**Fixed**	**Random**
Layout					
No EES	6.8	4.41	3.74	4.1	3.4
EES	1.21	1.72	1.23	0.96	0.71

However, using EES, the voltage variations are well reduced and met the requirement as regulated by the EN 50160 standard, and a WEP compliance level for safe grid connection can be ensured. The maximum voltage variation allowed at the PCC is ±10%, as defined in the standard EN 50160. Moreover, the power quality of the WEP was assessed for different layouts for different grid impedance angles in a fictitious grid. The PCC voltage was processed to obtain the flicker coefficients $c_f(\Psi_k)$ for Ψ_k : 30°, 50°, 70°, and 85°, and $S_k/S_p = 50$. c_f was determined as the 99th percentile of each set of $c_f(\Psi_k)$. The obtained results are presented in Table 2. The short-term flicker severity P_{st} is calculated for 600 s, and each time series was sampled and processed for 650 s at least. From the summarised results, it can be noted that in *Layout A*, where a single WEC was operating, barely met the grid code requirements for the flicker emissions P_{st} at the PCC without an energy storage. This condition feeds a poor power quality into the power grid. Hence, it is not relevant to integrate a single WEC to the grid of lower impedance angles, Ψ_k : 30°, 50°, 70° without an EES. However, the flicker level, P_{st}, flicker coefficients, c_f (see Table 2) and the voltage variation $\Delta V / V$ (see Table 1) are well below the limits allowed in other two layouts and meeting the grid compliance requirements by the standards IEC 61400-21 and EN 50160. In addition, the individual harmonics of the voltage at the PCC has been reduced from *Layout A* to *C* due to a significant reduction in the voltage variations and power pulsations. In *Layout A*, the THD content in the voltage is below the limits of 5.33% and 8% for very short-time and short-time values, respectively. The individual odd harmonics, third, fifth, seventh and ninth, and even harmonics, fourth, sixth and eighth, were found well within the limit of 5% at the time instants measured at 20, 100 and 200 s. The results were evaluated when using an EES and the confidence level for the 99th percentile very short time (3 s) values, 15 consecutive 10-cycle windows for the 50-Hz power system were fairly below the limit of 3.33% assigned by IEEE 519-2014 for individual harmonics, i.e. 1.5 times less of 5%. The results evaluated for the 95th percentile (10-min windows and for 200 consecutive very short time values) satisfied the requirements, as shown in bottom graph in Figure 7 in the blue bar. From the results in *Layouts B* and *C*, the individual harmonic contents were analysed for 95th percentile short-time values to determine the harmonic level at the PCC in different power penetrations. It can be noted from Figures 12 and 15 that the harmonic contents were significantly improved from *Layout B* to *C* due to the less voltage variations at the PCC. The results evaluated in both layouts (*B* and *C*) for different orientations of WECs satisfied the individual harmonic requirement (<5%)

of the WEP followed the grid compliance and grid code requirements in different orientations of the WEP for the given grid impedance level. Power and voltage variations are smoothed and reduced in the amplitude of variations to be compliant for a safe operation of the grid-connected WEP. Table 1 presents the maximum voltage variations for each layout at the PCC with a grid impedance angle of $\Psi_k = 70°$ (at the PCC of the test facility at the MaREI Centre).

TABLE 2 Flicker coefficients in *Layouts A, B* and *C* for different Ψ_k and $S_k/S_p = 50$ for the non-smoothed and smoothed powers

Ψ_k	Layout	*A* One WEC		*B*—three WECs Zero shift		10-s shift		*C*—10 WECs Fixed		Random	
		P_{st}	c_f	P_{st}	c_f	P_{st}	c_f	P_{st}	c_f	P_{st}	c_f
30°	No EES	0.82	41	0.23	11.5	0.17	8.5	0.089	4.6	0.067	3.35
	EES	0.18	9	0.081	4.1	0.05	2.5	0.047	2.35	0.038	1.9
50°	No EES	0.71	36	0.17	8.5	0.13	6.4	0.073	3.65	0.041	2.05
	EES	0.13	7	0.052	2.6	0.036	1.8	0.063	3.15	0.0081	0.40
70°	No EES	0.68	34	0.146	6.8	0.123	5.68	0.057	2.3	0.019	0.95
	EES	0.078	4	0.029	1.6	0.017	0.89	0.0079	0.41	0.0041	0.21
85°	No EES	0.29	15	0.056	2.8	0.07	3.5	0.067	3.4	0.014	0.7
	EES	0.03	1.5	0.009	0.46	0.007	0.35	0.017	0.9	0.0038	0.21
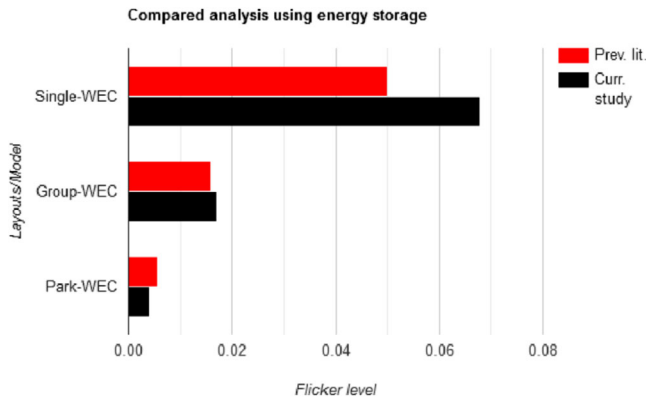
FIGURE 18 Grid impact of different models studied and compared to the previous study [11]

and THD requirement (<8%), as shown in Figures 13 and 16 for each phase of the voltage at the PCC. Therefore, from the investigated results, the recommended orientations that are grid compliant are 10-s shift in *Layout B* and random shift in *Layout C*. These two layouts are grid compliance without an EES for particular grid impedance angle and short-circuit ratio.

A compared analysis with previous literature is presented in Figure 18. The flicker level of different layouts is shown with the results presented by Trilla et al. [11] for a fictitious grid for a grid impedance angle of 70°. A single WEC model, a group model of three WECs in our case and a park model of 10 WECs in our case are compared to the results for approximately similar three models. Red bar presents the results from the previous literature, whereas black bar presents the results from this study. It is evident from a single WEC model that practicability of integration of one WEC is not a favourable condition. Moreover, a group model and a park model are significantly compliant to the grid codes due to a significant reduction in flicker severity. However, a small difference is noticeable in group model, but still both the orientations are grid compliant. Also, we can conclude that a park-based model with random shift is most favourable with an improved power quality. Moreover, it is worth to mention that the induced voltage variations, flicker levels and power fluctuations will depend on the design and type of WECs and PTO. The level of grid impact mitigation with and without WEPs is also an important factor to be addressed. This area is open for more discussions and research to achieve stable and improved wave energy from the oceans.

6 | CONCLUSION

This paper studied the grid impact of medium-size WEP in different layouts. The study focused in terms of flicker level at different power penetrations for a grid short-circuit ratio and impedance angle Ψ_k. The power system analysis was based on experimental power profiles of a linear-generator-based WEP and significant energy periods and wave heights recorded at the west coast of Sweden. The study compared the generated flicker level to the permitted limits as defined in the standard in a power quality context. In order to determine the WEP compliance compatibility, the flicker levels generated by the WEP in different power profiles and layouts were analysed. The induced individual harmonics and the THD at the PCC voltage were extensively analysed and compared to the limits. The study shows that the park consisting only single generator may have negative grid impact under certain conditions. However, the park consisting of three and 10 generators could be safely integrated with the AC power grid with a grid impedance angle of 70°. Since the power of the park is smaller than other studies in the present field, the grid short-circuit ratio becomes higher and supports the attenuation of the fluctuation at the PCC. It is worth to mention that the study was carried out in a variable-speed mode and found that the park is grid compliant in *Layout B*, 10-s shift and random case in *Layout C*, and followed the stringent limits for flicker emission enforced by the various grid operators. The harmonic distortion of the voltage in each phase was evaluated and considered grid code compliant in *Layouts B* and *C*. However, in *Layout A*, some type of energy storage would be required to meet the power quality demand enforced by the grid operators. The amplitude of the power pulsations

and voltage variations shown in different layouts predicted that the WEP integration to the grid compared to the wind parks can be achieved, since the power and voltage fluctuations occurred in lower frequency range of the WEP. The induced fluctuations can be mitigated by means of energy storages. At present, battery storage systems seem to provide a promising opportunity to mitigate the issues of load demand and power generation fluctuations in most applications. Moreover, this could increase the cost of the overall system due to the short life of the batteries caused by frequent charge and discharge cycles. Batteries present high energy density but low power density, servicing with a low charge/discharge rates. On the other hand, supercapacitors (SCs) are a versatile form of energy storage, which stores energy by means of static charge and used to compliment the battery in parallel as a hybrid energy storage system (HESS) [12]. A fully active HESS topology is a suitable solution to achieve an effective control over the battery and the SC currents. However, this presents individual characteristics in terms of energy and power density. Individual control becomes crucial to handle the power sharing over the battery and SC and control their state of charge especially, for the long life of the battery. This control topology protects the battery from high transients and reduces the losses, which ensures an enhancement of the battery life. As the SC is a high-power-density source, it can handle the high-frequency power components to reduce the stress on the battery. Hence, the overall maintenance and cost of the system can be reduced.

ACKNOWLEDGEMENTS

REFERENCES

1. Chiodo, E., Lauria, D., Pisani, C.: Wind farm production estimation under multivariate wind speed distribution. In: International Conference on Clean Electrical Power, pp. 745–750 (2013)
2. McArthur, S., Brekken, T.K.A.: Ocean wave power data generation for grid integration studies. In: IEEE PES General Meeting, pp. 1–6 (2010)
3. Sun, X., Huang, D., Wu, G.: The current state of offshore wind energy technology development. Energy, 41(1), 298–312 (2012)
4. Islam, M.R., Mekhilef, S., Saidur, R.: Progress and recent trends of wind energy technology. Renewable Sustainable Energy Rev., 21, 456–468 (2013)
5. Macpherson, D.E., Mueller, M.A., Shek, J.K.H.: Power conversion for wave energy applications. In: 5th IET International Conference on Power Electronics, Machines and Drives, pp. 1–6 (2010)
6. Sorensen, B.: Renewable Energy Conversion, Transmission, and Storage. Academic Press, New York (2007)
7. O'Sullivan, D.L., Dalton, G., Lewis, A.W.: Regulatory, technical and financial challenges in the grid connection of wave energy devices. IET Renewable Power Gener. 4, 555 (2010).
8. Tietje III, E.D.: International standards for the appraisal of wave energy converters. In: 'OCEANS 2009, pp. 1–5 (2009)
9. Gungor, V.C., et al.: Smart grid technologies: Communication technologies and standards. IEEE Trans. Ind. Inf. 7(4), 529–539 (2011)
10. Sharkey, F., et al.: Dynamic electrical ratings and the economics of capacity factor for wave energy converter arrays. In: European Wave and Tidal Energy Conference (2011)
11. Trilla, L., et al.: Wave energy park power quality impact and collection grid economic assessment. IET Renewable Power Gener. 9, 368–378 (2015)
12. Parwal, A., et al.: Energy management for a grid-connected wave energy park through a hybrid energy storage system. Appl. Energy 231(1), 399–411 (2018).
13. Hatziargyriou, N.: Microgrids: Architectures and Control. Wiley-IEEE Press, Hoboken (2013)
14. Cigre: Microgrids 1, Engineering, Economics, & Experience. Cigré, Paris (2015)
15. Kamel, R.M.: Hybrid and coordinated soft starting controller for wind generation system runs in the standalone micro grid. Sustainable Energy, Grids Networks, 5, 105–113 (2016)
16. Burmester, D., et al.: A review of nanogrid topologies and technologies. Renewable Sustainable Energy Rev., 67, 760–775 (2017)
17. Blavette, A., et al.: Impact of a medium-size wave farm on grids of different strength levels. IEEE Trans. Power Syst. 29, 917–923 (2014).
18. Blavette, A., et al.: Grid compliance of ocean energy converters: Control strategies and recommendations. In: 9th European Wave and Tidal Energy Conference (2011)
19. *IEEE Recommended Practice and Requirements for Harmonic Control in Electric Power Systems*, IEEE Std 519-2014 (2014)
20. *Measurement and Assessment of Power Quality Characteristics of Grid Connected Wind Turbines*. IEC 61400-21 (2001)
21. Moazzen, I., et al.: Impacts of large-scale wave integration into a transmission-constrained grid. Renewable Energy 88, 408-417 (2016).
22. Majidi Nezhad, M., et al.: Nearshore wave energy converters comparison and Mediterranean small island grid integration. Sustainable Energy Technol. Assess. 30, 68–76 (2018).
23. Alcorn, R.G.: Wave station modelling based on the islay prototype plant. Dissertation, Queen's University of Belfast (2000)
24. Redondo, K., et al: A strategy for improving the accuracy of flicker emission measurement from wind turbines. Electr. Power Syst. Res. 133, 12–19 (2016).
25. *Electromagnetic Compatibility (EMC)---Part 4–15: Testing and Measurement Techniques---Flickermeter---Functional and Design Specifications*. IEC 61000-4-15 (2010)
26. Nambiar, A.J., et al.: Effects of array configuration, network impacts and mitigation of arrays of wave energy converters connected to weak, rural electricity networks. In: 3rd International Conference on Ocean Energy, pp. 1–7 (2010)
27. Göteman, M., Engström, J., Eriksson, M., Isberg, J.: Optimizing wave energy parks with over 1000 interacting point-absorbers using an approximate analytical method. Int. J. Mar. Energy 10, 113–126 (2015).
28. Temiz, I., et al.: Power hardware-in-the-loop simulations of grid integration of a wave power park. In: 13th European Wave and Tidal Energy Conference, pp. 1–6 (2019)
29. Engström, J., et al.: Wave energy converter with enhanced amplitude response at frequencies coinciding with Swedish west coast sea states by use of a supplementary submerged body. J. Appl. Phys. 106(6), 064512 (2009)
30. Boström, C., et al.: Study of a wave energy converter connected to a non-linear load. IEEE J. Oceanic Eng., 34, 123–127 (2009)
31. Temiz, I., et al.: Economic aspects of latching control for a wave energy converter with a direct drive linear generator power take-off. Renewable Energy 128, 57–67 (2018).
32. Teodorescu, R., et al.: Proportional-resonant controllers and filters for grid-connected voltage-source converters. IEE Proc.—Electr. Power Appl. 153, 750–762 (2006).
33. McGranaghan, M., Beaulieu, G.: Update on IEC 61000-3-6: Harmonic emission limits for customers connected to MV, HV, and EHV. In: IEEE Power Engineering Society Transmission and Distribution Conference and Exhibition, pp. 1158–1161 (2006)
34. Fagan, E., et al.: Grid code provisions for wind generators in Ireland. In: IEEE Power Engineering Society General Meeting, pp. 1241–1247 (2005)

35. *Harmonisation of Balance Regulation in the Nordic Countries System*, NORDEL (2008)
36. Tedeschi, E., Santos-Mugica, M.: Modeling and control of a wave energy farm including energy storage for power quality enhancement: The bimep case study. IEEE Trans. Power Syst. 29(3), 1489–1497 (2014).
37. Miceli, R., Trapanese, M.: Evaluation of the power quality from a seawave power farm for different interconnection schemes. In: OCEANS 2007, pp. 1–4 (2007)
38. Cahill, B., Lewis, T.: Wave energy resource characterization and the evaluation of potential Wave Farm sites. In: OCEANS 2011, pp. 1–10 (2011)
39. Thiringer, T., Petru, T., Lundberg, S.: Flicker contribution from wind turbine installations. IEEE Trans. Energy Convers. 19, 157–163 (2004).
40. Monterrat, A., et al.: Grid integration for marine renewable energy devices in a real time application. In: 12th European Wave and Tidal Energy Conference, pp. 1–7 (2017)
41. Lundberg, S.: Electrical limiting factors for wind energy installations. Int. J. Renewable Energy Eng. 3(2), 305–310 (2000)
42. Ackermann, T.: Wind Power in Power Systems. Wiley, Hoboken (2005)
43. Ruiz, J., Lazkano, A., Leturiondo, L.A.: Measurement of voltage flicker: Application to grid-connected wind turbines. In: Advances in Measurement Systems. InTech, Rijeka (2012)
44. Markiewicz, H., Klajn, A.: Voltage characteristics of electricity supplied by public distribution systems, pp. 2–5 (2004)
45. Glover, J.D., Sarma, M.S., Overbye, T.: Power System Analysis and Design. Thomson, Australia (2008)

APPENDIX
Appendix A: Tuned parameters of PR + HC controller

	Parameters	Symbols	Values
PR controller	Proportional gain	K_P	6.3
	Integral gain	K_i	1501.14
	Resonant frequency	ω	314.16 rad/s
	Bandwidth frequency	ω_c	0.5 rad/s
HC controller	Third resonant frequency	3ω	942.48 rad/s (150 Hz)
	Integral gain	K_i	201.11
	Bandwidth frequency	ω_c	3.1 rad/s
	Fifth resonant frequency	5ω	1570.8 rad/s (250 Hz)
	Integral gain	K_i	81.154
	Bandwidth frequency	ω_c	5.2 rad/s
	Seventh resonant frequency	7ω	2199.11 rad/s (350 Hz)
	Integral gain	K_i	39.786
	Bandwidth frequency	ω_c	10 rad/s

Appendix B: Parameters of microgrid and its components

	Parameters	Symbols	Values
Microgrid parameters At PCC	Voltage line–line	V_{ll}	400 V
	Frequency	f_g	50 Hz
	Grid-impedance angle	Ψ_k	70°
Inverter parameters (VSI)	Switching frequency	f_s	10 kHz
	Series inductance	L_i	3.9 mH
	Shunt capacitance	C_f	20 μF
	Active-gain	k_ω	13.3
	Reactive gain	k_E	186
WEC side converter	Switching frequency	f_s	3 kHz
	Proportional gain	K_P	68.8
	Integral gain	K_i	1746.4
DC link	Capacitor voltage	V_{dc}	650 V
	Capacitance	C_{dc}	50 mF
EES: Li-ion battery	Rated capacity	$P_{t-\mathrm{BAT}}$	5 kWh
	Rated-charging current	$I_{\mathrm{dc-ch}}$	34 A
	Rated-discharge current	$I_{\mathrm{dc-dch}}$	18 A
	DC–DC converter switching frequency	$f_{\mathrm{sw-dc}}$	5 kHz

Appendix C: A running setup at MaREI Centre facility showing the measured/referenced torque, speed, and other parameters of motor drive and generator drive in the HIL test system. Measured voltages and currents at different nodes are shown. A green round symbol on connection lines specifies a closed connection, while a red symbol is for open connection. Courtesy, MaREI.